Reversible 2'-OH Acylation Enhances RNA Stability

Eric Kool (kool@stanford.edu)
Stanford University https://orcid.org/0000-0002-7310-2935
Linglan Fang
Stanford University https://orcid.org/0000-0003-2637-090X
Lu Xiao
Stanford University
Yong Woong Jun
Yoshiyuki Onishi
Stanford University

Article

Keywords:

Posted Date: April 26th, 2022

DOI: https://doi.org/10.21203/rs.3.rs-1483354/v1

Reversible 2'-OH Acylation Enhances RNA Stability

Linglan Fang, Lu Xiao, Yong Woong Jun, Yoshiyuki Onishi, and Eric T. Kool*
Department of Chemistry and ChEM-H Institute, Stanford University, Stanford, CA 94305
*Author to whom correspondence should be addressed: kool@stanford.edu

Stabilization of RNAs for storage, transport, and biological application remains a serious challenge, particularly for larger RNAs that are not accessible by chemical synthesis. Here, we present reversible 2'-OH acylation as a general strategy to preserve RNA of any length or origin. High-yield polyacylation of 2'-hydroxyls ("cloaking") by readily accessible acylimidazole reagents effectively shields RNAs from both thermal and enzymatic degradation. Subsequent treatment with water-soluble nucleophilic reagents removes acylation adducts quantitatively ("uncloaking") and recovers a remarkably broad range of RNA functions, including reverse transcription, translation, and gene editing. Furthermore, we show that certain α-dimethylamino- and α-alkoxy- acyl adducts are spontaneously removed in human cells, restoring mRNA translation with extended functional half-lives. These findings support the potential of reversible 2'-acylation as a simple and general molecular solution for enhancing RNA stability, and provide mechanistic insights for stabilizing RNA regardless of length or origin.

The thermal and enzymatic instability of RNA presents profound challenges to RNA vaccines and therapies, imposing severe limits on RNA analysis, storage and transportation, and pharmacology[1,2]. RNA degradation is pervasive and arises both from spontaneous thermal degradation and from the action of adventitious ribonuclease enzymes[3]. The predominant mechanism of RNA degradation starts with the attack of the deprotonated 2′-hydroxyl group on the vicinal 3′-phosphate, coordinated with the departure of the adjacent 5′-alcohol and resulting in 2′,3′-cyclic phosphate (**Fig. 1a**)[3,4]. The same mechanism, aided by general acids and bases in the ribonuclease active site, also underlies RNA premature degradation by nuclease enzymes (*e.g.*, RNases) that are ubiquitously present in cells and biofluids[2,5], limiting half-lives of bioactive RNAs employed in therapeutic strategies[6,7].

Current methods to preserve RNA include the incorporation of modified inter-nucleotide linkages (*e.g.*, phosphorothioate[8], methylphosphonate[9], chemically altered nucleotides (*e.g.*, 2'-O-methoxy (2'-OMe)[10], 2'-O-methoxyethyl (2'-MOE)[11], and 2'-fluoro (2'-F)[12]), modified ribose (*e.g.*, locked nucleic acid (LNA)[13]), and structure-guided sequence design[7]. While these chemical modifications and sequence optimization have been widely employed to enhance RNA stability, their broad application is in most cases limited to short chemically synthesized RNA and can impart significant labor and expenses. Therefore, finding cost-effective strategies to preserve and subsequently restore RNA of any origin post-synthetically under mild conditions could constitute a major advance in RNA technologies in general, and facilitate the storage and therapeutic use of a broad range of biologically active RNAs.

Given the central role of the 2'-OH group in RNA cleavage, RNA degradation could in principle be blocked by post-synthetic acylation of these groups in RNA. Surprisingly, although acylation chemistry for mapping RNA structure has been studied for some time, few if any studies exist that exploit the chemical reversibility of 2'-carboxyl esters for high-yield reversible RNA protection. Numerous chemical reagents, such as anhydrides and acyl chlorides have been described for 2'-hydroxyl covalent modification[14-16]. However, the short aqueous half-lives and poor water solubility of reagents with these functional groups limit the extent of RNA modification. More recently, two newer chemotypes have been developed to overcome these issues; alkylamino-substituted isatoic anhydrides[17,18] and acylimidazoles[19,20] can survive longer in water and react in high yields with RNA. We were attracted to acylation by acylimidazoles due to their simplicity, their ease of preparation, high water solubility, and their effective RNA 2'-polyacylation ability (**Fig. 1b**). We recently demonstrated that acylimidazoles can efficiently react with 2'-hydroxyls rather than exocyclic amines on nucleobases[21] and exhibit tunable hydrolytic half-lives[22]. Acylimidazoles are easily accessible by one-step activation of the corresponding carboxylic acids with equimolar 1,1'-carbonyldiimidazole (CDI). Moreover, the 2'-carboxyl ester adducts with RNA can be reversed by design, offering a possible solution to reinstate unmodified 2'-hydroxyls[21-24]. These properties led us to consider the possibility that acylimidazoles might offer a simple solution to reversibly functionalize 2'-hydroxyls and block RNA degradation before biological use (**Fig. 1c**).

Here, we demonstrate that reversible 2'-hydroxyl acylation by newly designed acylimidazole reagents can broadly protect RNA from thermal and enzymatic degradation. The regioselective, high-yield reaction between 2'-hydroxyls and water-soluble acylimidazoles ("cloaking") affords 2'-polyacylation of a wide range of RNAs, ranging from short synthetic RNAs to long endogenous messenger RNAs. Using a set of readily accessible acylimidazoles that are structurally diversified, we surveyed how 2'-polyacylation of RNA influences its thermal and enzymatic instability. Further, we describe the discovery of water-soluble nucleophilic reagents that can efficiently remove selected acylation adducts ("uncloaking") and restore RNA functions, including reverse transcription, translation, and gene editing. Finally, we report that certain acylation adducts are reversed spontaneously in cells and restore mRNA translation with extended functional half-lives. Taken together, our reversible acylation reagents and methods represent a simple and broadly applicable post-synthetic strategy to preserve and subsequently recover RNA activity.

Results and discussion

RNA cloaking by acylimidazoles shields RNA from thermal degradation. RNAs (particularly longer RNAs) are susceptible to chain cleavage in water accelerated by thermal motions[25,26]. We first prepared a 2'-polyacylated ("cloaked") model mRNA by reacting a well-studied eGFP-mRNA (996nt) with NAI-N_3 (**1**), an acylimidazole reagent known to selectively acylate 2'-hydroxyls in high yields (**Fig. 1d**)[20]. MALDI-TOF analyses with an 18nt model RNA determined reaction conditions that provide intermediate (~50%) and extensive (>90%) cloaking (**Extended Data Fig. S1**). These conditions were used to generate modified eGFP-mRNA with an estimated half or nearly all of 2'-hydroxyls cloaked by **1**, further documented by its reduced electrophoretic mobility (**Extended Data Fig. S2**).

As an initial assessment of how cloaking affects the stability

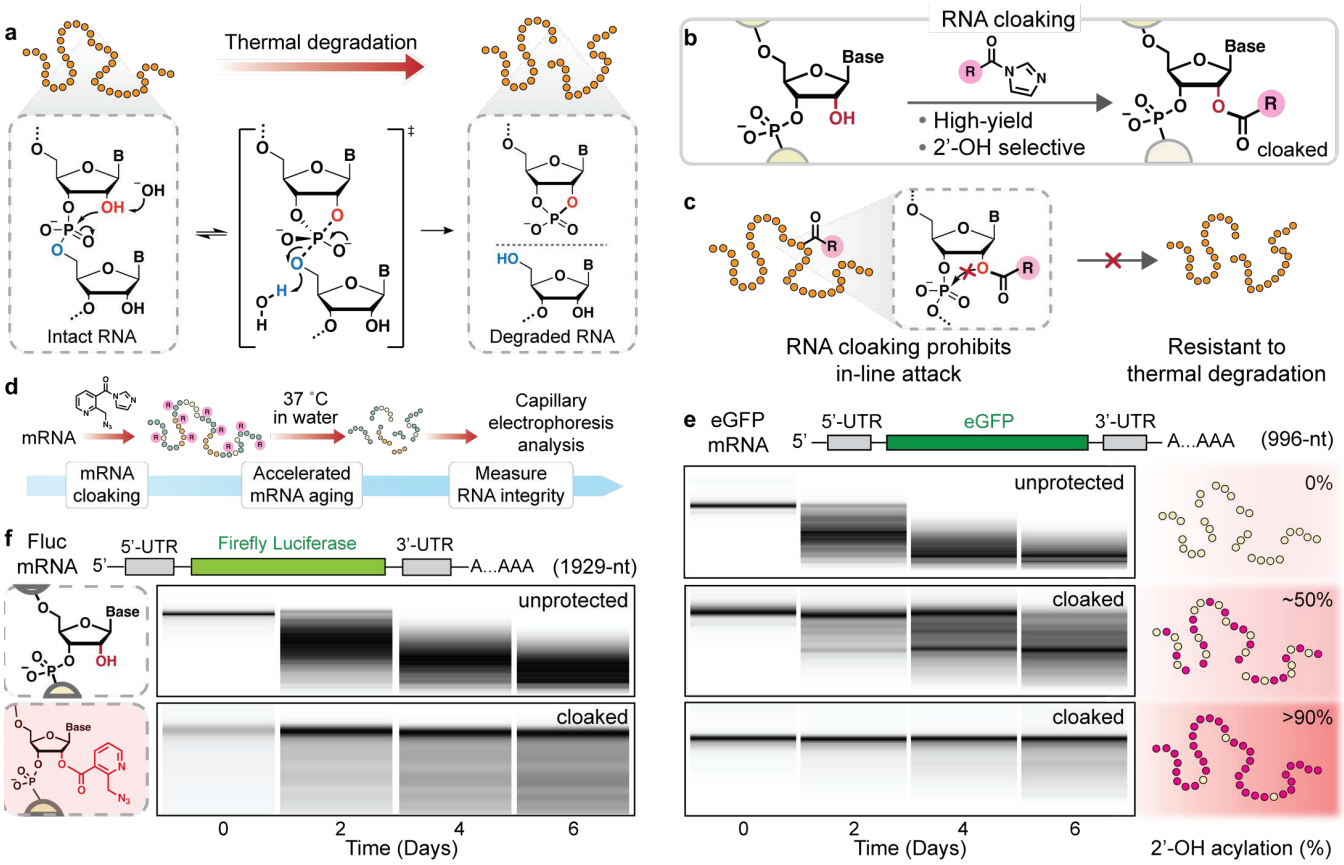

Fig. 1 | RNA polyacylation (cloaking) inhibits thermal degradation of RNA. a, Molecular mechanism of RNA thermal degradation in solution. **b**, Acylimidazole reagents cloak RNA in high yields post-synthetically. **c**, Cloaked RNA resists thermal degradation in solution by blocking nucleophilic 2'-hydroxyls from attacking the vicinal 3'-phosphodiester bonds. **d**, Experimental workflow to determine thermal stability (water, 37 ˚C) of mRNA cloaked with NAI-N_3 (**1**) with capillary electrophoresis (CE) analysis. **e-f**, The apparent RNA quality (measured by CE) of eGFP-mRNA (**e**) and Fluc-mRNA (**f**) cloaked with **1** upon incubation in RNase-free water over time. **e**, eGFP-mRNA tested was unprotected (top), intermediately (~50%, middle) or extensively (>90%, bottom) cloaked with **1**. **f**, Fluc-mRNA tested was either unprotected (top) or extensively (>90%, bottom) cloaked with **1**. Data shown are images of CE traces.

of RNA, we performed accelerated RNA aging experiments by incubating eGFP-mRNA species with or without cloaking in RNase-free water at a mildly elevated temperature (37 ˚C) (**Fig. 1d**). RNA cloaking was initially performed with acylimidazole **1** for 4 h. We then measured the lifespan of the fully intact mRNA. Analysis by capillary electrophoresis (CE) of RNA fragments showed cloaking-dependent resistance to RNA degradation (**Fig. 1e**); for instance, intermediate cloaking (~50%) extended the lifespan of intact eGFP-mRNA by ~3-fold, while extensive cloaking (>90%) was capable of near-complete shielding this RNA from thermal cleavage, with only <13% degradation after six days. Acylation-induced stabilization was further tested on a second, longer mRNA (FLuc-mRNA, **Fig. 1f**). As before, extensive cloaking (>90%) also almost completely blocked backbone cleavage of Fluc-mRNA over six days in water (37°C).

Structurally diverse acylimidazole agents enhance RNA stability in solution. Next, we explored whether the physico-chemical features of acylimidazole reagents can affect their abilities to suppress RNA thermal degradation. We prepared a panel of six additional acylimidazole reagents containing structurally diversified substituents intended to afford preliminary structure-activity relationships (**Fig. 2a**). These library reagents were readily prepared with one-step activation of their corresponding carboxylic acids by 1,1'-carbonyldiimidazole (**Extended Data Fig. S3a**). In the design of library compounds, we also paid attention to the installation of heteroatoms proximal to the carboxyl center, which we hypothesized would later facilitate the nucleophile-promoted hydrolysis ("uncloaking") to restore RNA. MALDI-TOF analyses determined reaction conditions for each reagent (**2-7**) to provide intermediate (~50% of 2'-hydroxyls) cloaking using the model RNA (**Extended Data Fig. S1**).

We screened these acylimidazole reagents for modulation of RNA thermal degradation by performing accelerated RNA aging experiments with eGFP-mRNA aliquots that were equivalently cloaked (~50%) with reagents **2-7** (**Fig. 2b**). Representative CE data are shown in **Fig. 2d-i** for eGFP-mRNA cloaked with **2-7**, which resisted thermal degradation across broad substituent types. The smallest (acetylimidazole, **3**) was notable as it attenuated RNA hydrolysis despite lacking a bulky aromatic substituent (**Fig. 2e**). Other active alkyl acylimidazoles (**4-7**) also greatly augmented RNA thermal stability, with ethoxyacetyl compound **6** providing the most stability to eGFP-mRNA (**Fig. 2f-i**). Noting subtle differences in the stabilization, we hypothesized that the varying protection afforded by the reagents might arise from differential hydrolytic stability of their adducts; this was later confirmed (see below). For example, the slightly reduced enhancement of RNA thermal stability by *N*,*N*-dimethylglycine (DMG) derivative **4** is likely due to faster hydrolysis of DMG-ester at elevated temperatures[27] (**Fig. 2f**), reflecting possible inductive effects and intramolecular general acid facilitation by its protonated tertiary amine[28]. Taken together, the data confirm that ester adducts of acylimidazoles

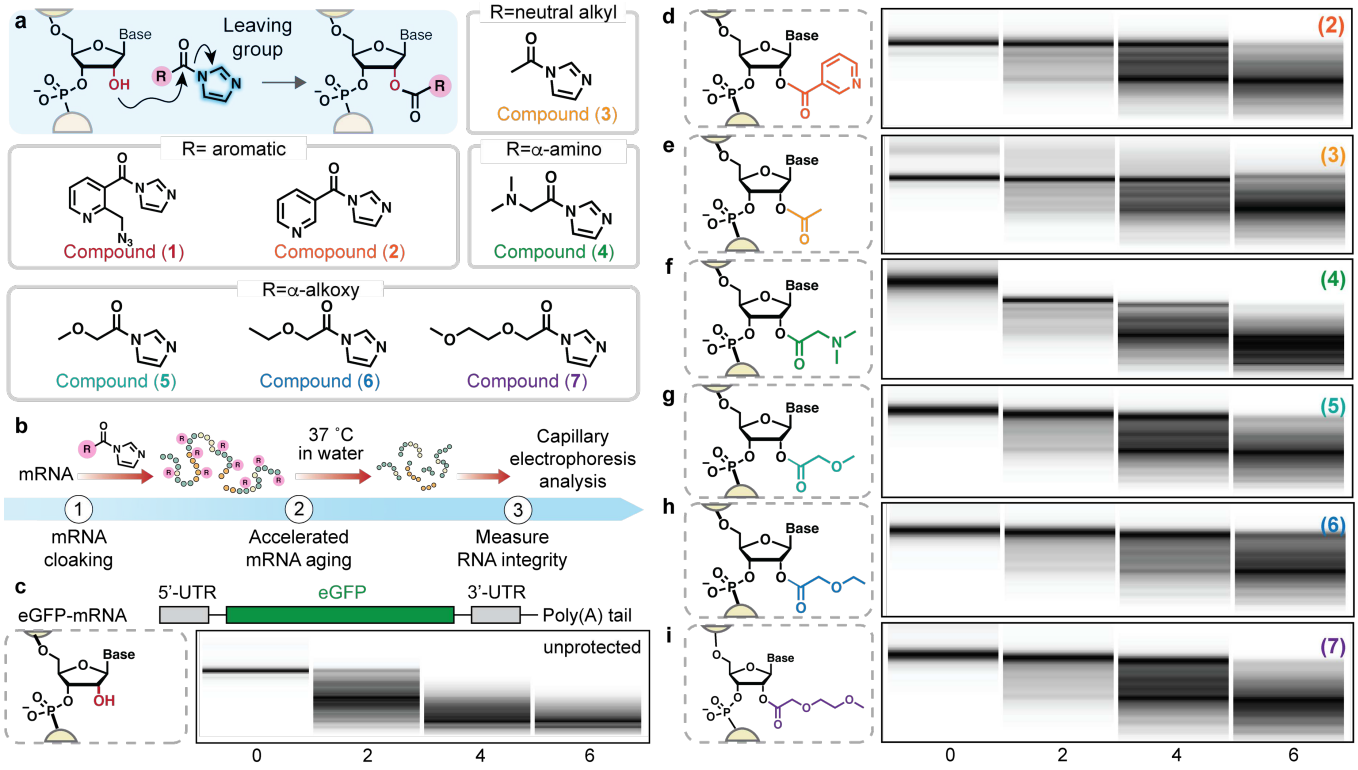

Fig. 2 | Structurally diverse acylimidazole reagents enhance RNA stability in solution. a, Structures of acylimidazole agents **1**-**7** clustered by the size and electronic properties. **b**, Experimental workflow to determine the thermal stability of cloaked mRNA with CE analysis. **c**-**i**, Qualitative assessment of the apparent RNA quality of unprotected eGFP-mRNA (**c**), or eGFP-mRNA intermediately cloaked by **2** (**d**), **3** (**e**), **4** (**f**), **5** (**g**), **6** (**h**), or **7** (**i**) upon incubation in RNase-free water over time (37 ˚C). Data shown are images of CE traces.

block RNA thermal degradation, and this general stabilizing effect appears to be independent of size and aliphatic versus aromatic construction.

RNA cloaking suppresses enzymatic RNA degradation by RNases and biofluids. In principle, acylimidazoles can enhance enzymatic stability of RNA by protecting phosphodiester linkages from RNase-mediated attacks by 2'-hydroxyls (**Fig. 3a**). Thus, we next surveyed protective effects with representative RNases and biofluids, recapitulating the common enzymatic conditions RNAs encounter during storage, handling, and application. As an initial assessment, we performed RNA degradation experiments with a 25nt model RNA that was extensively cloaked with the benchmark acylimidazole NAI-N_3 (**1**) (**Fig. 3b-c**; see **Extended Data Fig. S4a-b** for PAGE gel analyses). We found that RNA cloaking by **1** effectively shielded cleavage sites on the model RNA from nucleolytic degradation by RNase A—the prototypical member of RNase A superfamily abundant in vertebrate tissues[29-31], and RNase T1—a representative ssRNA-cleaving endonuclease[32]. In contrast, the unprotected RNA was almost completely cleaved. Because RNase A-type ribonucleases account for 70-80% of total ribonuclease activity in blood serum[33], we next evaluated whether cloaking could ameliorate RNA degradation in fetal bovine serum (FBS), a frequent component of eukaryotic cell culture. Consistent with the reported short lifespan of RNA in blood (<15 seconds in human serum)[34], the unprotected RNA was completely digested immediately upon contact with fetal bovine serum (FBS) (**Fig. 3c** and **Extended Data Fig. S4c**). In contrast, extensive cloaking by **1** attenuated RNA degradation. Since the target RNA strand was exposed to an excessive amount of serum, the observed degradation of the extensively cloaked RNA likely stems from serum RNases cleaving the RNA backbone near 2'-OH groups that remained unprotected. Finally, we also found that cloaking with **1** effectively stabilized the underlying RNA in human cell lysates (**Fig. 3c**), suggesting possible future uses in stabilizing RNAs intracellularly.

Varied acylimidazole agents attenuate sgRNA degradation by RNases. To explore whether protection against enzymatic degradation by cloaking extended beyond short RNAs, we characterized how acylimidazoles affect enzymatic degradation of EMX1-sgRNA, a 105nt single guide RNA (sgRNA) for CRISPR-Cas9 gene editing (**Fig. 3d**). We screened representative acylimidazoles for their effects on RNA enzymatic stability by performing RNA aging experiments with EMX1-sgRNA that was equivalently cloaked (~50%) with these reagents (**Fig. 3e**). The resistance to RNases was independent of the aromaticity of acyl groups (**Fig. 3f-g**). Consistent with unprotected 2'-OH being susceptible to RNase degradation, we found that decreased levels of cloaking by **4** and **5** led to expectedly lower RNase T1 resistance. Extending this further, a similar resistance profile was observed for extensively cloaked sgRNA in RNase-rich serum (**Fig. 3h**), strongly suggesting that extensive RNA cloaking provided resistance to a broad range of RNases. Interestingly, an intermediate level of cloaking by **4**-**5** facilitated rather than suppressed RNA cleavage by FBS; a possible hypothesis is that intermediate cloaking unwinds double-stranded regions of EMX1-sgRNA that were otherwise inaccessible by RNases.

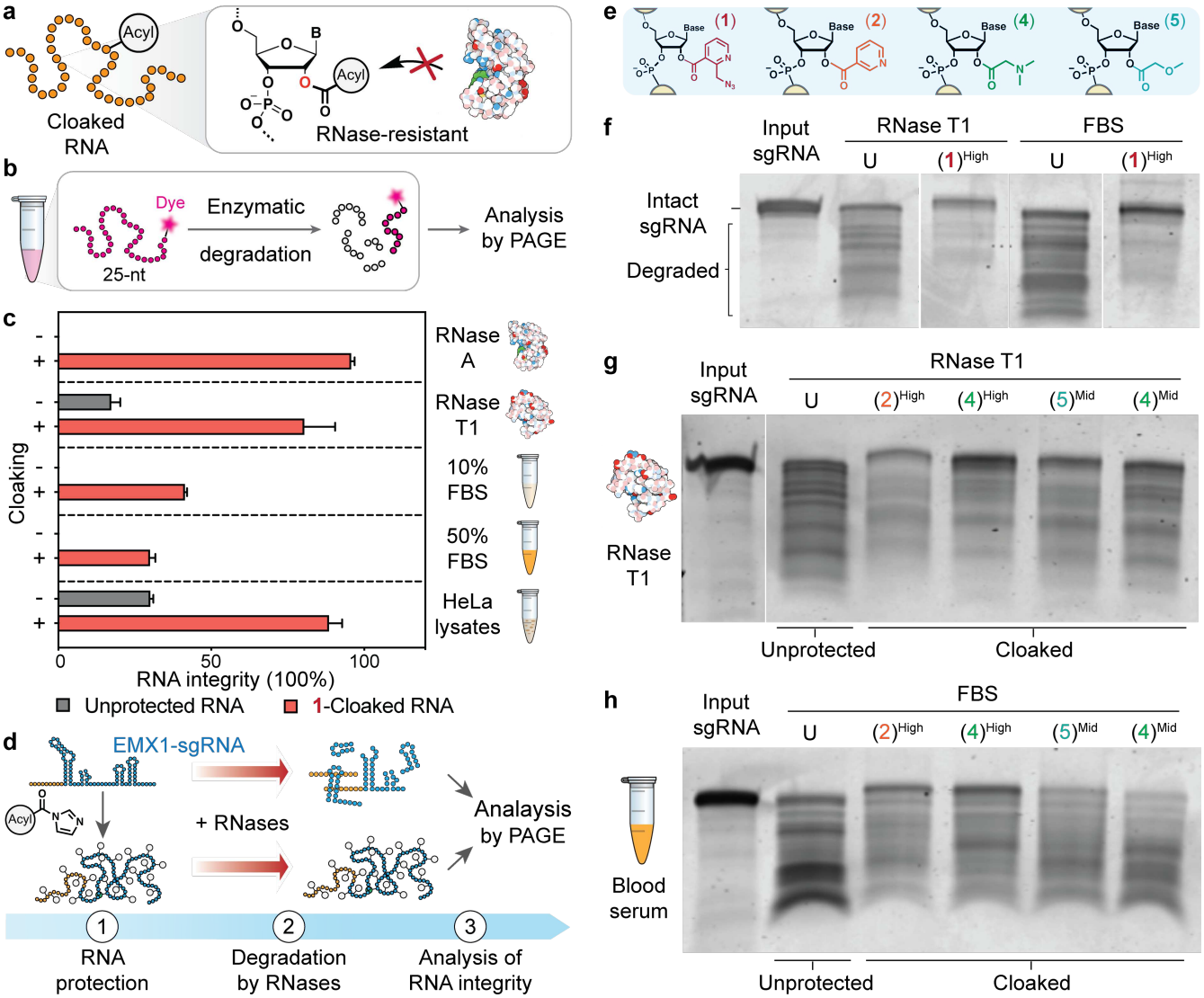

Fig. 3 | RNA cloaking suppresses enzymatic RNA degradation by RNases and biofluids. **a**, RNA cloaking confers resistance to degradation by RNases. **b**, Experimental workflow to quantify RNA integrity of a 25nt Dye-labeled model RNA after treatment with RNA-degrading enzymes and biofluids. **c**, Plot comparing the integrity of the model RNA after treatment with designated RNA-degrading conditions. RNA is unprotected or extensively cloaked with acylimidazole **1**. Data represent mean ± s.e.m., *n*=3. **d**, Experimental workflow to evaluate the resistance of cloaked 105nt EMX1-sgRNA against RNases. **e**, Molecular structures of 2'-acylated nucleotides by **1**, **2**, **4**, or **5**. **f**, Representative PAGE gel showing cloaking-dependent blockage of sgRNA degradation by RNase T1 and FBS *in vitro* (U: unprotected). **g-h**, Representative PAGE gel showing the impacts of acylimidazole and level of cloaking on sgRNA degradation by RNase T1 (**g**) and FBS (**h**) *in vitro*. For **f-h**, the experiments were conducted twice with similar results. *High* indicates high level of RNA cloaking (estimated >90%), while *Mid* indicates intermediate level (estimated ~50%).

Nucleophilic reagents remove 2'-polyacylation to uncloak RNA. Nucleophiles are known to catalyze ester hydrolysis; examples include the use of imidazole and pyridine as nucleophilic catalysts[35]. To restore biological activity of RNAs after cloaking-based stabilization, we tested uncloaking strategies to promote rapid hydrolysis of 2'-carboxyl esters with weakly basic nucleophiles (**Fig. 4a**). To this end, we assembled a panel of 13 reagents that were known as strong nucleophiles or promoters of ester hydrolysis[36], with pKa values ranging from ~10 to 9.7 (**Fig. 4b**). In the library design, we avoided the use of strong Brønsted bases to prevent hydrolytic RNA backbone cleavage[37]. Nucleophiles were screened against the 18nt model RNA containing acyl groups of each type at 37 ˚C and neutral pH, which identified at least 9 sensitive acylation-nucleophile pairs that promoted >50% removal of adducts within 2 hours (**Fig. 4c-h** and **Extended Data Fig. S5**).

Comparing the sensitivities of 2'-acyl adducts towards each nucleophile, we found a strong correlation with the physico-chemical properties. Aromatic acyl groups tended to show greater resistance towards nucleophile-promoted hydrolysis in general (**Fig. 4d** and **Extended Data Fig. S5b**), possibly due to their steric bulk. Aliphatic adducts showed distinct sensitivities towards library nucleophiles. For 2'-acyl adduct by **4**, the effects of the biocompatible tris(hydroxymethyl)aminomethane (Tris) buffer alone were substantial, consistent with previous reports that Tris can hydrolyze active esters[38,39] (**Fig. 4e-f**). Interestingly, and in contrast, the simple acetyl adducts by acetylimidazole (**3**) were not reversed by Tris, nor by any of the other conditions tested (**Extended Data Fig. S5c**), strongly suggesting that the heteroatom at the α-carbon of DMG derivative **4** sensitizes the ester for hydrolysis. Notably, α-alkoxyesters of **5**-**7** displayed major differences in their vulnerabilities towards nucleophiles compared to the DMG ester, showing that the heteroatom

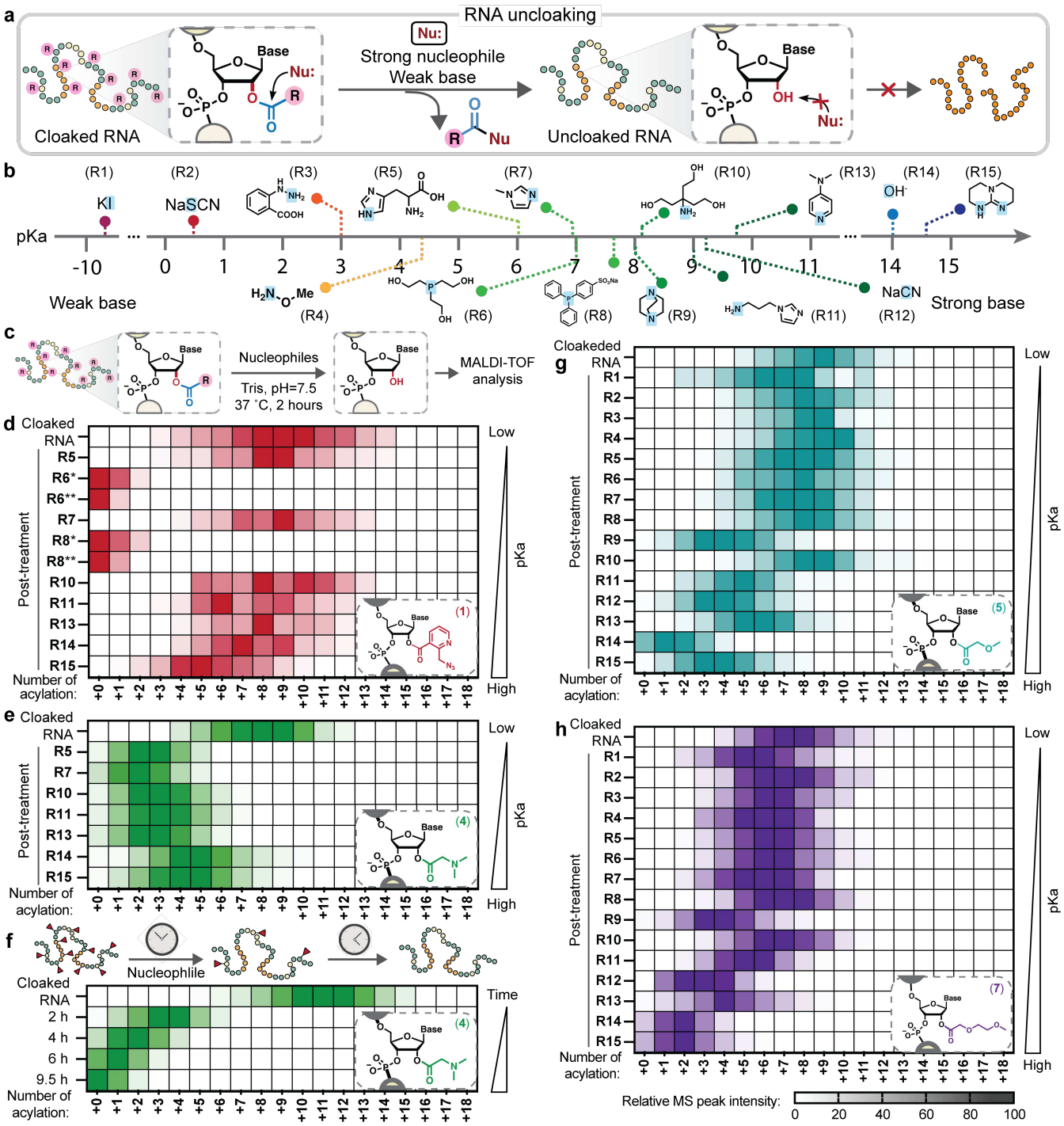

Fig. 4 | Nucleophilic reagents remove 2'-polyacylation to uncloak RNA. a, General strategy for RNA uncloaking by nucleophile-facilitated hydrolysis of 2'-carboxyl esters. **b**, Chemical structures of 13 nonbasic nucleophilic reagents (**R1**-**R13**) ranked by the pKa of their conjugate acids (electrophilic centers highlighted in blue). **c**, Experimental workflow to screen nucleophiles for RNA uncloaking with an 18nt model RNA. MALDI-TOF analysis quantifies the efficiency of 2'-ester hydrolysis. **d**-**e**, Heat map comparing the hydrolysis rate of 2'-carboxyl esters by various nonbasic nucleophiles at pH 7.5 (50 mM, 2 h, 37 ˚C). Model RNA was cloaked by acylimidazole reagents **1** (**d**) and **4** (**e**). * and **: Phosphines reverse 2'-acylation by **1** via Staudinger reductions[23]. **f**, Quantitative assessment of the apparent hydrolytic rate of 2'-acyl adduct by acylimidazole **4** in Tris buffer at pH 7.5 (50 mM, 37 ˚C), as measured by MALDI-TOF. **g**-**h**, Heat map comparing the hydrolysis of 2'-carboxyl esters by nonbasic nucleophiles at pH 7.5 (50 mM, 2h, 37 ˚C). Model RNA was cloaked by acylimidazole reagents **5** (**g**) and **7** (**h**). In **d**-**h**, heat map represents the number of remaining 2'-acyl adducts per RNA.

substitution at the α-carbon can significantly modulate an ester's susceptibility towards nucleophiles (**Fig. 4g-h** and **Extended Data Fig. S5d**).

Nucleophile-promoted RNA uncloaking restores RNA functions. Although our nucleophilic reagents could restore a relatively short RNA, a practical challenge remained; namely, whether these reagents could be employed to recover much longer and more sensitive RNAs while keeping the strands intact and functional. For instance, the ability of a single 2'-acylation to halt reverse transcriptase during primer extension necessitates efficient 2'-deacylation to avoid premature reverse transcription

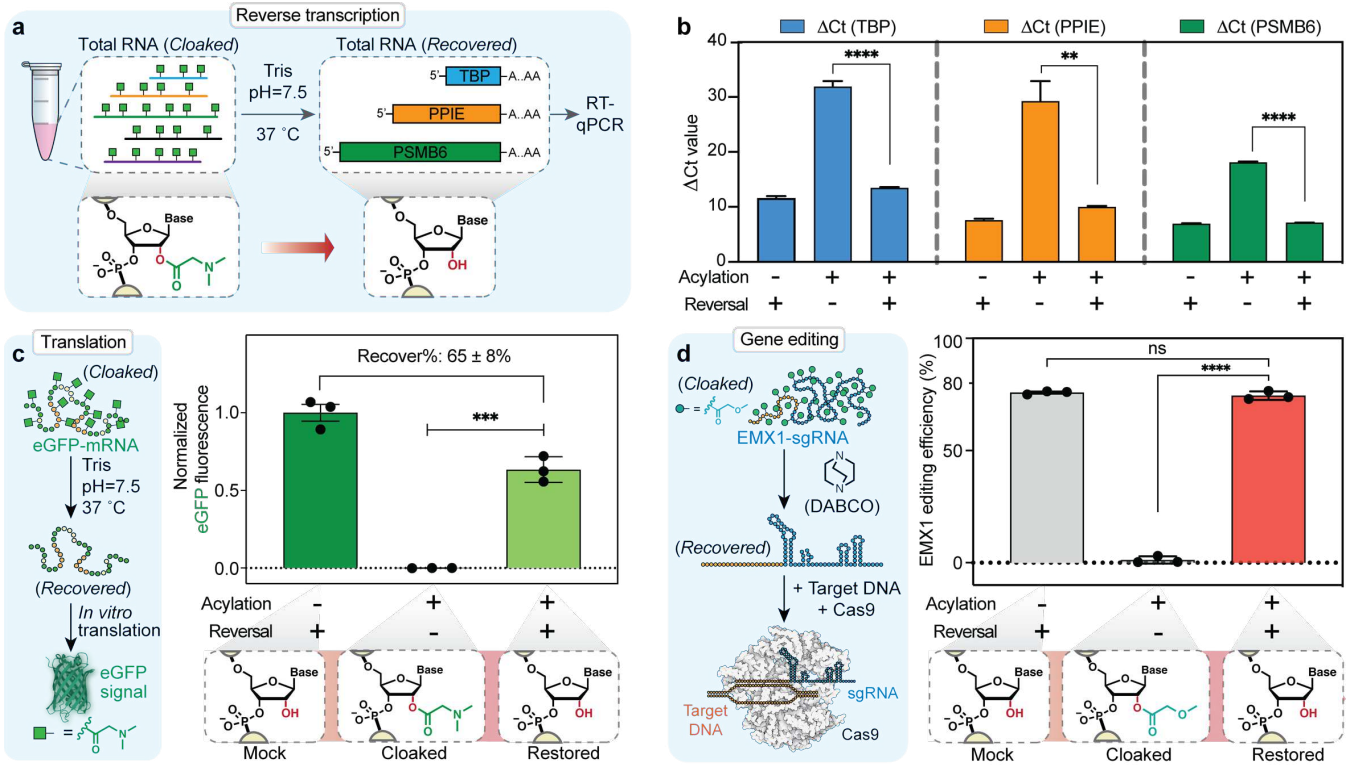

Fig. 5 | Nucleophile-promoted RNA uncloaking restores RNA functions. a, Experimental workflow to restore reversible transcription of **4**-cloaked cellular mRNA with Tris buffer alone. **b**, Bar graph comparing the ΔCt values for three representative isolated cellular mRNA before and after uncloaking by Tris. *P* values shown were <0.0001 (TBP), 0.0063 (PPIE), and <0.0001 (PMSB6). **c**, Experimental workflow to restore translation of DMG-cloaked eGFP-mRNA with Tris (left panel) and bar graphs comparing eGFP expression before and after uncloaking by Tris (right panel). *P* value shown was 0.0002. **d**, Experimental workflow to recover gene-editing function of EMX1-sgRNA with DABCO (left panel) and bar graph comparing the efficiency of EMX1-sgRNA-mediated dsDNA breakage before and after uncloaking by DABCO (right panel). *P* value shown was <0.0001. In **b**, **c**, and **d**, data represent mean ± s.e.m., *n*=3 of three biologically independent experiments. Statistical significance was calculated with two-tailed Student's *t*-tests: ***P*<0.01, ****P*<0.001, *****P*<0.0001.

termination[20]. Accordingly, we assessed whether these nucleophiles could restore reverse transcription (RT) of acylated RNA. We isolated and cloaked total cellular RNA from HEK293 cells with reagent **4**, and recovery efficiency was evaluated for three representative mRNAs by the reverse transcription efficiencies. RT-qPCR results in **Fig. 5a-b** showed that incubation with Tris alone at neutral pH reinstated the reverse transcription of the cloaked mRNAs (TBP, PPIE, and PSMB6) after 24 h, regardless of their transcript and amplicon lengths. Additionally, the restored cellular RNA demonstrated similar or the same ΔCt values compared to their unprotected counterparts, establishing that RNA uncloaking by Tris is biocompatible for effective recovery of reverse transcription of diverse RNAs.

Recent experiments have shown that 2'-acylation can terminate translation when introduced into the coding region of mRNAs[40,41]. Thus, we characterized whether Tris could restore the translation of a model eGFP-mRNA densely cloaked by **4**. Based on *in vitro* translation assays (**Fig. 5c**), intermediate cloaking with **4** strongly blocked the translation of eGFP-mRNA, while treatment with 50 mM Tris, pH=7.5 at 37 ˚C leads to 65±7% restoration of eGFP expression. Electrophoresis experiments (**Extended Data Fig. S6**) showed that the mRNA integrity remained largely unchanged. These data suggested that Tris alone could recover mRNA translation of adducts of **4**, while keeping the RNA intact. To explore the generality of this observation, we applied the methods to a CRISPR sgRNA[24,42]. Acylation of EMX1-sgRNA by **5** fully blocked its cleavage function (<1%) *in vitro* (**Fig. 5d**). Treatment of **5**-cloaked sgRNA with 50 mM of 1,4-diazabicyclo[2.2.2]octane (DABCO) at neutral pH for 8 hours fully restored DNA cleavage.

Spontaneous RNA uncloaking in human cells restores mRNA translation with extended functional half-lives. Intact cells maintain high intracellular concentrations of nucleophilic species such as cysteine and glutathione. The sensitivity observed here of 2'-carboxyl esters towards nucleophilic hydrolysis suggests possibility of spontaneous RNA uncloaking both during and after cellular delivery, which might enable RNA functional recovery (**Fig. 6a**). To explore this possibility, we employed cloaked mRNAs encoding fluorescent reporter proteins. Indeed, we observed the emergence of strong green fluorescence signals by flow cytometry over a period of two days in HeLa cells transfected with intermediately **4**-cloaked eGFP-mRNA (**Fig. 6b**). Single-blind fluorescence imaging further confirmed that the translation of **4**-cloaked eGFP-mRNA was restored after an initial delay compared to its unprotected counterpart (**Fig. 6c-d**), corroborating the spontaneous RNA uncloaking in live cells. In marked contrast, for eGFP-mRNA that was cloaked with **1**, translation remained strongly inhibited (**Extended Data, Fig. S7a**). This further confirmed that the recovery of eGFP expression is due to the releasing properties of DMG-ester of **4**, and testing in two additional cell lines (SW480, HEK293) confirmed generality (**Fig. 6e-f**). Moreover, the delayed translation of cloaked mRNAs reflects an initial uncloaking step, which when occurring over time may provide slow-release translation kinetics—reducing an early expression peak and extending the duration of translation (see below). Finally, we also observed that translation of eGFP-mRNA with α-alkoxyl acyl adduct (**7**) can also be restored in cells, highlighting possible control over mRNA release kinetics by modification of the acyl group (**Extended Data Fig. S7b**).

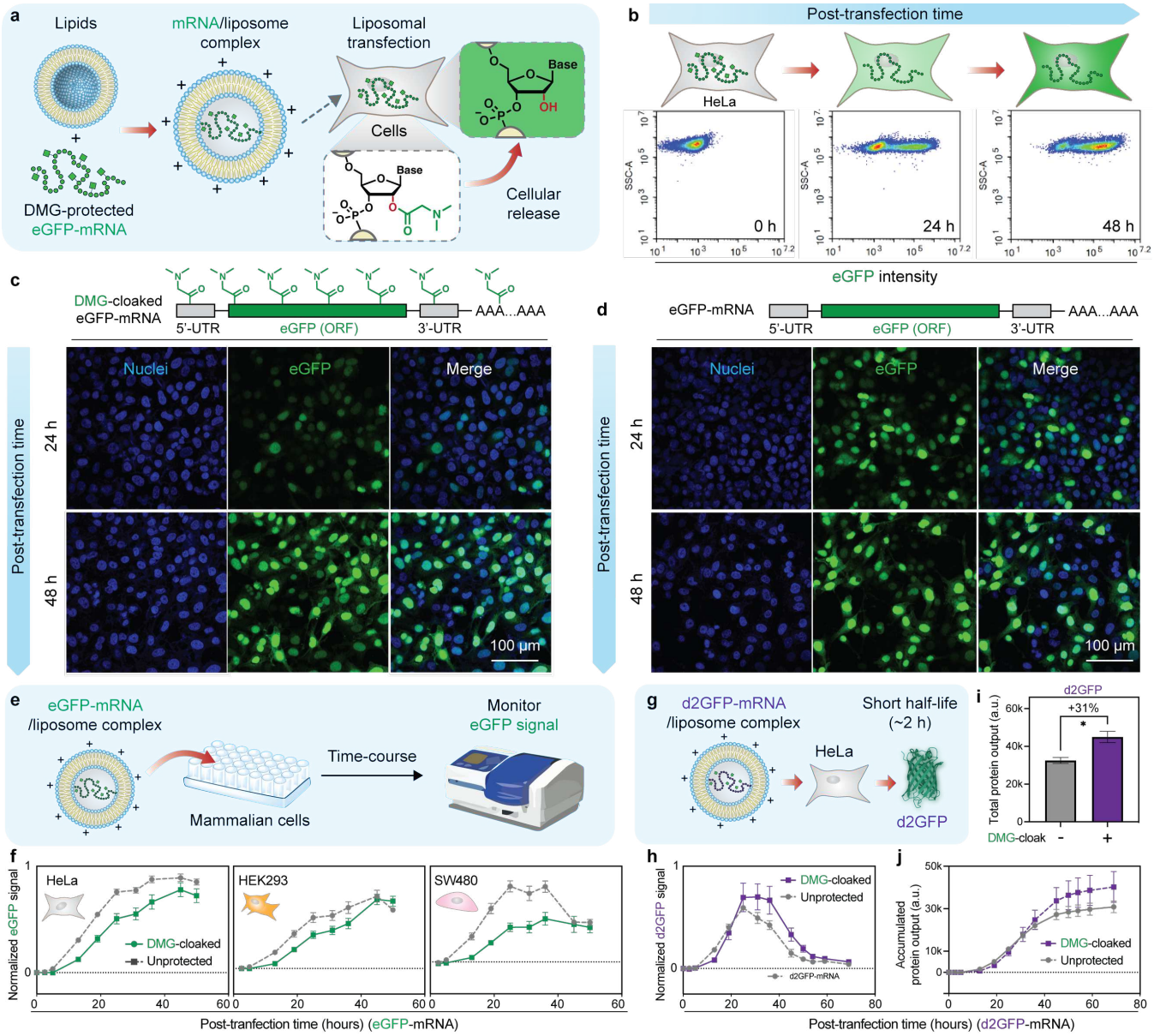

Fig. 6 | Spontaneous RNA uncloaking restores mRNA translation with extended functional half-lives in human cells. **a**, General schematic for liposomal delivery of cloaked mRNA to spontaneously release mRNA and restore translation in cells. **b**, FACS analysis determines eGFP expression of HeLa cells transfected with **4**-cloaked eGFP-RNA over two days. **c**-**d**, Representative single-blind fluorescence micrographs of HeLa cells transfected with **4**-cloaked eGFP-mRNA (**c**) and unprotected eGFP-mRNA (**d**) at 24 h and 48 h. **e**, Schematic for a fluorimeter-based assay to measure the kinetics of eGFP-mRNA translation. **f**, **4**-Cloaked eGFP-mRNA translates in HeLa (left panel), HEK293 (middle panel), and SW480 (right panel) cells. **g**, Liposomal transfection of d2GFP-mRNA in HeLa cells. **h**, Cloaking by **4** extended the translation of d2GFP-mRNA in HeLa cells. **i**, Cloaking by 4 enhanced the total protein output of d2GFP-mRNA after 69 h. **j**, Accumulated protein output of d2GFP-mRNA with or without cloaking by **4** at indicated timepoints. In **f** and **h**-**j**, data represent mean ± s.e.m., *n*=3 per group from three biologically independent experiments.

We next investigated how cloaking affects the functional lifespan of mRNA in cells. Because eGFP protein is highly stable with a half-life >24 hours[43], protein degradation alone dominates expression and provides no information about mRNA functional half-lives[44]. We therefore adopted a reporter system employing mRNA encoding a destabilized green fluorescent protein d2GFP, where both mRNA and protein degradation occur with similar half-lives of ~2-3 hours (**Fig. 6g**)[44,45]. We observed that the translation of unprotected d2GFP-mRNA quickly descended after peaking (**Fig. 6h**). In contrast, intermediate cloaking by **4** led to sustained d2GFP-mRNA translation at its peak level for ~10 hours, strongly suggesting its ability to extend the functional lifespan of d2GFP-mRNA effectively. This extended mRNA functional half-life also enhanced the total protein output of d2GFP-mRNA by 31% in HeLa cells (**Fig. 6i**) and this enhancement became increasingly prominent after ~31 h post-transfection compared to unprotected d2GFP-mRNA (**Fig. 6j**). Taken together, RNA cloaking by DMG derivative **4** effectively extended d2GFP-mRNA functional lifespan and translation, providing insights for future use of reversible 2'-acylation as a general modulator of mRNA translation kinetics.

Conclusions

We have shown that RNA cloaking by reversible 2'-hydroxyl acylation effectively enhances the thermal and nucleolytic stability of a wide range of RNAs. The high-yield cloaking by water-soluble acylimidazoles can be broadly applied in one step to RNA of any origin, making it a remarkably simple and general

strategy for RNA preservation. We note that the marked enhancement of RNA half-lives presents strong implications for improved RNA storage and could ease the need for costly ultracold conditions. Further increases in RNA half-lives through cloaking are likely possible, as resistance towards thermal degradation depends on the hydrolytic stability of 2'-acyl adducts, which can be tuned. Furthermore, cell-permeable acylimidazoles can acylate RNA in tissues[20], suggesting future utility of these features during RNA isolation for biomolecular or clinical studies.

To restore biological activity after storage, efficient unblocking of RNAs is necessary. We have shown that water-soluble nucleophiles can reverse 2'-acylation to restore numerous RNA functions. We find that 2'-α-alkoxyesters are sensitive to multiple nucleophiles, and the DMG-ester adducts of **4** are especially sensitive to nucleophiles including Tris buffer (pH 7.5). Notably, other buffers lacking the primary amine of Tris such as MOPS and HEPES, do not facilitate hydrolysis of DMG ester at physiological pH (**Extended Data Fig. S5f**). These data suggest structure-specific features of Tris that preferentially promote DMG-ester hydrolysis[35,38,39]. Additional mechanistic studies of new nucleophile analogues will be useful in exploring this hypothesis in the future.

Our kinetics studies provide first-in-class evidence regarding the application of RNA cloaking for extended release of RNA functions in cells. We find that the translation of **4**-cloaked eGFP-mRNA was initiated after a ~7-hour delay compared to its unprotected counterpart, which reflects the existence of in-cell deacylation processes. Presumably, active 2'-carboxyl esters are sensitive to certain nucleophilic groups in cells and/or in the intraparticle space of LNPs[46,47], resulting in rapid recovery of the underlying RNA, although the precise uncloaking mechanism remains under investigation. Another useful feature of RNA cloaking is the ability to increase mRNA functional half-lives in cells. We showed that cloaking by **4** extended the peak d2GFP-mRNA translation by ~10 hours, >3-fold of the reported half-life of unmodified d2GFP-mRNA (3 hours)[48], and enabled greater overall protein expression. Understanding this phenomenon will provide new mechanistic insights into future efforts to leverage 2'-modifications for modulating RNA pharmacokinetics.

References

1. Fabre, A. L., Colotte, M., Luis, A., Tuffet, S. & Bonnet, J. An efficient method for long-term room temperature storage of RNA. *Eur J Hum Genet* **22**, 379-385 (2014).
2. Wayment-Steele, H. K. *et al.* Theoretical basis for stabilizing messenger RNA through secondary structure design. *Nucleic Acids Res* **49**, 10604-10617 (2021).
3. Kellerman, D. L., York, D. M., Piccirilli, J. A. & Harris, M. E. Altered (transition) states: mechanisms of solution and enzyme catalyzed RNA 2'-O-transphosphorylation. *Curr Opin Chem Biol* **21**, 96-102 (2014).
4. Guo, F. *et al.* Effect of Ribose Conformation on RNA Cleavage via Internal Transesterification. *J Am Chem Soc* **140**, 11893-11897 (2018).
5. Breslow, R. & Chapman, W. H., Jr. On the mechanism of action of ribonuclease A: relevance of enzymatic studies with a p-nitrophenylphosphate ester and a thiophosphate ester. *Proc Natl Acad Sci U S A* **93**, 10018-10021 (1996).
6. Lee, J. B., Hong, J., Bonner, D. K., Poon, Z. & Hammond, P. T. Self-assembled RNA interference microsponges for efficient siRNA delivery. *Nat Mater* **11**, 316-322 (2012).
7. Leppek, K. *et al.* Combinatorial optimization of mRNA structure, stability, and translation for RNA-based therapeutics. *bioRxiv* (2021).
8. Hendel, A. *et al.* Chemically modified guide RNAs enhance CRISPR-Cas genome editing in human primary cells. *Nat Biotechnol* **33**, 985-989 (2015).
9. Miller, P. S. *et al.* Nonionic nucleic acid analogues. Synthesis and characterization of dideoxyribonucleoside methylphosphonates. *Biochemistry* **18**, 5134-5143 (1979).
10. Wu, S. Y. *et al.* 2'-OMe-phosphorodithioate-modified siRNAs show increased loading into the RISC complex and enhanced anti-tumour activity. *Nat Commun* **5**, 3459 (2014).
11. Korobeynikov, V. A., Lyashchenko, A. K., Blanco-Redondo, B., Jafar-Nejad, P. & Shneider, N. A. Antisense oligonucleotide silencing of FUS expression as a therapeutic approach in amyotrophic lateral sclerosis. *Nat Med* **28**, 104-116 (2022).
12. Yin, H. *et al.* Structure-guided chemical modification of guide RNA enables potent non-viral in vivo genome editing. *Nat Biotechnol* **35**, 1179-1187 (2017).
13. Guinea-Viniegra, J. *et al.* Targeting miR-21 to treat psoriasis. *Sci Transl Med* **6**, 225re221 (2014).
14. Ovodov, S. & Alakhov Yu, B. mRNA acetylated at 2'-OH-groups of ribose residues is functionally active in the cell-free translation system from wheat embryos. *FEBS Lett* **270**, 111-114 (1990).
15. Goldsborough, S. Modified polynucleotides and uses thereof. US patent US 2003/0039985 A1 (2003).
16. Steen, K. A., Siegfried, N. A. & Weeks, K. M. Selective 2'-hydroxyl acylation analyzed by protection from exoribonuclease (RNase-detected SHAPE) for direct analysis of covalent adducts and of nucleotide flexibility in RNA. *Nat Protoc* **6**, 1683-1694 (2011).
17. Fessler, A. B. *et al.* Water-Soluble Isatoic Anhydrides: A Platform for RNA-SHAPE Analysis and Protein Bioconjugation. *Bioconjug Chem* **29**, 3196-3202 (2018).
18. Fessler, A. B., Fowler, A. J. & Ogle, C. A. Directly Quantifiable Biotinylation Using a Water-Soluble Isatoic Anhydride Platform. *Bioconjug Chem* **32**, 904-908 (2021).
19. Velema, W. A. & Kool, E. T. The chemistry and applications of RNA 2'-OH acylation. *Nat Rev Chem* **4**, 22-37 (2020).
20. Spitale, R. C. *et al.* Structural imprints in vivo decode RNA regulatory mechanisms. *Nature* **519**, 486-490 (2015).
21. Velema, W. A., Kietrys, A. M. & Kool, E. T. RNA Control by Photoreversible Acylation. *J Am Chem Soc* **140**, 3491-3495 (2018).
22. Park, H. S., Kietrys, A. M. & Kool, E. T. Simple alkanoyl acylating agents for reversible RNA functionalization and control. *Chem Commun (Camb)* **55**, 5135-5138 (2019).
23. Kadina, A., Kietrys, A. M. & Kool, E. T. RNA Cloaking by Reversible Acylation. *Angew Chem Int Ed Engl* **57**, 3059-3063 (2018).
24. Habibian, M. *et al.* Reversible RNA acylation for control of CRISPR-Cas9 gene editing. *Chem Sci* **11**, 1011-1016 (2019).
25. Li, Y. & Breaker, R. R. Kinetics of RNA Degradation by Specific Base Catalysis of Transesterification Involving the 2'-Hydroxyl Group. *Journal of the American Chemical Society* **121**, 5364-5372 (1999).
26. Soukup, G. A. & Breaker, R. R. Relationship between internucleotide linkage geometry and the stability of RNA. *RNA* **5**, 1308-1325 (1999).
27. Takata, J. *et al.* Vitamin K prodrugs: 1. Synthesis of amino acid esters of menahydroquinone-4 and enzymatic reconversion to an active form. *Pharm Res* **12**, 18-23 (1995).
28. Johnson, S. L. in *Advances in Physical Organic Chemistry* Vol. 5 (ed V. Gold) 237-330 (Academic Press, 1967).
29. delCardayre, S. B. & Raines, R. T. Structural determinants of enzymatic processivity. *Biochemistry* **33**, 6031-6037 (1994).
30. Raines, R. T. Ribonuclease A. *Chem Rev* **98**, 1045-1066 (1998).

31. Garnett, E. R. & Raines, R. T. Emerging biological functions of ribonuclease 1 and angiogenin. *Crit Rev Biochem Mol Biol*, 1-17 (2021).
32. Pace, C. N., Heinemann, U., Hahn, U. & Saenger, W. Ribonuclease T1: Structure, Function, and Stability. *Angewandte Chemie International Edition in English* **30**, 343-360 (1991).
33. Sorrentino, S., Naddeo, M., Russo, A. & D'Alessio, G. Degradation of double-stranded RNA by human pancreatic ribonuclease: crucial role of noncatalytic basic amino acid residues. *Biochemistry* **42**, 10182-10190 (2003).
34. Tsui, N. B., Ng, E. K. & Lo, Y. M. Stability of endogenous and added RNA in blood specimens, serum, and plasma. *Clin Chem* **48**, 1647-1653 (2002).
35. Jencks, W. P. & Carriuolo, J. Reactivity of Nucleophilic Reagents toward Esters. *Journal of the American Chemical Society* **82**, 1778-1786 (1960).
36. van der Helm, M. P., Klemm, B. & Eelkema, R. Organocatalysis in aqueous media. *Nature Reviews Chemistry* **3**, 491-508 (2019).
37. Jarvinen, P., Oivanen, M. & Lonnberg, H. Interconversion and phosphoester hydrolysis of 2',5'- and 3',5'-dinucleoside monophosphates: kinetics and mechanisms. *The Journal of Organic Chemistry* **56**, 5396-5401 (1991).
38. Werber, M. M. & Shalitin, Y. The reaction of tertiary amino alcohols with active esters: I. Acylation and deacylation steps. *Bioorganic Chemistry* **2**, 202-220 (1973).
39. de Jersey, J., Fihelly, A. K. & Zerner, B. On the mechanism of the reaction of tris(hydroxymethyl)aminomethane with activated carbonyl compounds: A model for the serine proteinases. *Bioorganic Chemistry* **9**, 153-162 (1980).
40. Xiao, L., Jun, Y. W. & Kool, E. T. DNA Tiling Enables Precise Acylation-Based Labeling and Control of mRNA. *Angew Chem Int Ed Engl* **60**, 26798-26805 (2021).
41. Park, H. S., Jash, B., Xiao, L., Jun, Y. W. & Kool, E. T. Control of RNA with quinone methide reversible acylating reagents. *Org Biomol Chem* **19**, 8367-8376 (2021).
42. Wang, S. R. *et al.* Conditional control of RNA-guided nucleic acid cleavage and gene editing. *Nat Commun* **11**, 91 (2020).
43. Kain, S. R. Green fluorescent protein (GFP): applications in cell-based assays for drug discovery. *Drug Discov Today* **4**, 304-312 (1999).
44. Singh, A., Razooky, B. S., Dar, R. D. & Weinberger, L. S. Dynamics of protein noise can distinguish between alternate sources of gene-expression variability. *Mol Syst Biol* **8**, 607 (2012).
45. Li, X. *et al.* Generation of destabilized green fluorescent protein as a transcription reporter. *J Biol Chem* **273**, 34970-34975 (1998).
46. LoPachin, R. M. & Gavin, T. Reactions of electrophiles with nucleophilic thiolate sites: relevance to pathophysiological mechanisms and remediation. *Free Radic Res* **50**, 195-205 (2016).
47. Hou, X., Zaks, T., Langer, R. & Dong, Y. Lipid nanoparticles for mRNA delivery. *Nat Rev Mater* **6**, 1078-1094 (2021).
48. Raj, A., Peskin, C. S., Tranchina, D., Vargas, D. Y. & Tyagi, S. Stochastic mRNA synthesis in mammalian cells. *PLoS Biol* **4**, e309 (2006).
49. Gu, C. *et al.* Chemical synthesis of stimuli-responsive guide RNA for conditional control of CRISPR-Cas9 gene editing. *Chem Sci* **12**, 9934-9945 (2021).
50. Warren, L. *et al.* Highly efficient reprogramming to pluripotency and directed differentiation of human cells with synthetic modified mRNA. *Cell Stem Cell* **7**, 618-630 (2010).

Methods

Materials. DNA and RNA were purchased from IDT, TriLink BioTechnology, or Stanford PAN facility unless otherwise stated (see Supplementary Table 1 for details). All chemicals purchased from commercial suppliers were used without further purification (see Supplementary Table 2 for details). All enzymes, kits, bioreagents, and software were obtained from sources listed in Supplementary Table 2. Human cell lines HEK293 (CRL-1573), HeLa (CRM-CCL-2), and SW480 (CCL-228) were purchased from American Type Culture Collection (ATCC) and maintained in DMEM supplemented with 10% FBS at 37 ˚C in a humidified incubator containing 5% CO_2.

Synthesis of acylimidazole reagents (1-7). Reagent **1** was synthesized according to previously reported protocols[20]. Reagents **2**-**7** were synthesized with the following general protocol: The carboxylic acid precursor (1.0 equiv.) was dissolved in dry DMSO as a 4 M solution. To it was added an equal volume of a suspension containing 1.0 equivalent of 1,1'-Carbonyldiimidazole at room temperature. The resulting solution was stirred at room temperature for 4 hours. After the reaction, the final solution can be stored and used as a 2 M acylimidazole stock without further purification. The chemical structures of acylimidazole reagents were verified by ^{1}H-NMR and ^{13}C-NMR spectroscopy (see Supplementary Information for detailed compound-specific synthetic protocols).

Generation of EMX1-sgRNA and d2GFP-mRNA. The template for *in vitro* transcription (IVT) of EMX1-sgRNA was generated according to previously reported protocols[49]. EMX1-sgRNA was then synthesized through IVT with the HiScribe™ T7 High Yield RNA Synthesis Kit (NEB, E2040S) according to the manufacturer's protocol. The IVT template of d2GFP-mRNA was cloned according to previously reported protocols[50]. d2GFP-mRNA was then generated through IVT with the HiScribe™ T7 High Yield RNA Synthesis Kit according to the manufacturer's protocol. The resulting mRNA was capped with Vaccinia Capping System according to manufacturer's protocol. See Supplementary Table 1 for related oligonucleotides sequences.

RNA purification by ethanol precipitation. The reaction solution was diluted to 100 µL with RNase-free water. 10 µL of 3 M NaOAc (pH=5.5) and 1 µL of RNA-grade glycogen (20 µg/µL) was added and mixed by vortexing. Next, 500 µL of ice-cold 96% ethanol was added and mixed by vortexing. The resulting mixture was incubated at -80 ˚C overnight and then centrifuged at 21,100*g* for 40 mins to pellet. The pellet was washed with 200 µL ice-cold 70% ethanol once and air-dried for 15 mins. RNA was reconstituted with RNase-free water.

RNA cloaking. The cloaked RNAs were generated by reacting RNAs with acylimidazole reagents in aqueous solutions. After cloaking, short RNAs (tRF-3005 RNA and IR700-RNA) were purified by precipitation with ethanol as described above. The other RNAs (EMX1-sgRNA, eGFP-mRNA, d2GFP-mRNA, Fluc-mRNA, and total cellular RNA) were purified with RNA Cleanup & Concentrator Column-5 according to the manufacturer's protocol.

To generate intermediately (~50%) **1**-cloaked RNA, 500 ng of RNA (tRF-3005 RNA, IR700-RNA, EMX1-sgRNA, or eGFP-mRNA) was diluted into an 8 µL solution with RNase-free water. 2 µL of 750 mM stock of **1** in DMSO was then added to the RNA solution. The reaction mixture was then incubated at room temperature for 4 hours. To generate extensively (>90%) **1**-cloaked RNA, 500 ng of RNA (tRF-3005 RNA, IR700-RNA, EMX1-sgRNA, eGFP-mRNA, or Fluc-mRNA) was diluted into an 8 µL solution with RNase-free water. 2 µL of 1.5 M stock of **1** in DMSO was then added to the RNA solution. The mixture was incubated at 37 ˚C for 4 hours.

To generate intermediately (~50%) **2**-cloaked RNA, 500 ng of RNA (tRF-3005 RNA or eGFP-mRNA) was diluted into an 8 µL solution with RNase-free water. 2 µL of 1 M stock of **2** in DMSO was then added to the RNA solution. The mixture was incubated at room temperature for 4 hours. To generate extensively (>90%) **1**-cloaked RNA, 2.5 µg of RNA (EMX1-sgRNA) was diluted into a 35 µL solution with RNase-free water. 15 µL of 1.33 M stock of **2** in DMSO was then added to the RNA solution. The mixture was incubated at 37 ˚C for 4 hours.

To generate intermediately (~50%) **3**-cloaked RNA, 500 ng of RNA (tRF-3005 RNA) was diluted into an 8 µL solution with RNase-free water. 2 µL of 2 M stock of **3** in DMSO was then added to the RNA solution. The mixture was incubated at room temperature for 4 hours.

To generate intermediately (~50%) **4**-cloaked RNA, 500 ng of RNA (tRF-3005 RNA, eGFP-mRNA, EMX1-sgRNA, d2GFP-mRNA, or total cellular RNA) was diluted into an 8 µL solution containing 700 mM HEPES, pH=7.3 and chilled on ice for >5 mins. 2 µL of 500 mM stock of **4** in DMSO was then added to the RNA solution. The mixture was incubated at 4 ˚C for 2.5 hours. To generate extensively (>90%) **4**-cloaked RNA (tRF-3005 RNA or EMX1-sgRNA), 2.5 µg of RNA was diluted into a 40 µL solution containing 700 mM HEPES, pH=7.3 and chilled on ice for >5 mins. 10 µL of 2 M stock of **4** in DMSO was then added to the RNA solution. The mixture was incubated at 4 ˚C for 2.5 hours.

To generate intermediately (~50%) cloaked RNA by **5**-**7**, 1.5 µg of RNA (tRF-3005 RNA, eGFP-mRNA, EMX1-sgRNA, or d2GFP-mRNA) was diluted into an 18 µL solution with RNase-free water and chilled on ice for >5 mins. 9 µL of 2 M stock of **5**-**7** in DMSO was then added to the RNA solution. The mixture was incubated at 4 ˚C for 4 hours.

Screening of nonbasic nucleophiles for RNA uncloaking. 5 µL of cloaked tRF-3005 RNA (~15 µM) was mixed with 3 µL of 3.3×reaction buffer (165 mM Tris, pH=7.5). 2 µL of reversal solution in water was then added, which contains 250 mM of nonbasic nucleophiles including potassium iodide (KI, in water), sodium thiocyanate (NaSCN, in water), 2-hydrazino benzoic acid (in DMSO), methoxyamine-HCl (in DMSO), histidine (in water), sodium 3-(diphenylphosphino) benzenesulfonate (TPPMS, in water), Tris(hydroxypropyl)phosphine (THPP, in water), 1-methyl imidazole (in DMSO), 1,4-diazabicyclo[2.2.2]octane (DABCO, in water), tris(hydroxymethyl)aminomethane (Tris, pH=7.5), 3-aminopropylimidazole (DMAP, in DMSO), sodium cyanate (NaCN, in water), 4-dimethylaminopyridine (DMAP, in water). The resulting solution was incubated at 37 ˚C for 2 hours. The RNA was purified by precipitation with ethanol according to the protocol described above. 7 µL of RNase-free water was added to dissolve the resulting RNA pellet and reconstitute the RNA solution. The remaining number of 2'-acyl adducts were determined with MALDI-TOF analyses. Reactions were performed for one time per condition.

RNA uncloaking. To uncloaked total cellular RNA, 1 µg of **4**-cloaked isolated cellular RNA was diluted into 10 µL with

RNase-free water. 10 μL of 100 mM Tris, pH=7.5 was then added to the reaction. The resulting solution was incubated at 37 ˚C for 24 hours. Upon completion, the uncloaked total cellular RNA was used in the RT-qPCR experiments without further purification.

To uncloak eGFP-mRNA, 2 μL of 50 ng/μL **4**-cloaked eGFP-mRNA was diluted with 3 μL with RNase-free water. 5 μL of 100 mM Tris, pH=7.5 was then added to the reaction. The resulting solution was incubated at 37 ˚C for 24 hours. Upon completion, the solution was used in the following *in vitro* translation experiments without further purification.

To uncloak EMX1-sgRNA, 1 μg of **5**-cloaked EMX1-sgRNA was first diluted into a 14 μL solution with water, then mixed with 5 μL of 250 mM Tris (pH 7.5), 5 μL of 250 mM DABCO, and 1 μL of RiboLock. The resulting solution was incubated at 37 ˚C for 9 hours and then used in CRISPR-Cas9 experiments without further purification.

Determine RNA thermal stability with accelerated mRNA aging experiments. Two model long mRNAs (eGFP-mRNA and Fluc-mRNA) were used to evaluate the thermal stability of cloaked RNA. 50 μL of a solution containing 10 ng/μL of mRNA species in RNase-free water was incubated in a sealed RNase-free PCR tube at 37 ˚C. After 2, 4, and 6 days, 3 μL of the mRNA solution was collected at each time point and RNA integrity was analyzed by capillary electrophoresis (CE) on Agilent RNA 6000 Pico Chips using an Agilent 2100 Bioanalyzer. CE data were processed and visualized using 2100 Expert software (Agilent). CE traces are shown in **Fig**. **1**-**2**.

Determine RNA enzymatic stability of IR700-25nt RNA. (Protection of RNA from RNase A) A solution of 1×PBS, pH=7.4 containing 1 pmol of IR700-25nt RNA (unmodified or cloaked) and RNase A (1.0 μg/mL) was incubated at 37 ˚C for 45 mins. (Protection of RNA from RNase T1) A 10 μL solution of reaction buffer (50 mM Tris, pH=7.5 + 1 mM EDTA) containing 1 pmol of IR700-25nt RNA (unmodified or cloaked) and RNase T1 (0.5 U/μL) was incubated at 37 ˚C for 45 mins. (Protection of RNA from FBS) A 10 μL solution of 1×PBS, pH=7.4 containing 1 pmol of IR700-25nt RNA (unmodified or cloaked) and 10% (or 50%) FBS were incubated at 37 ˚C for 2 mins; (Protection of RNA from HeLa lysates) A 10 μL solution of 1 mg/mL HeLa lysates in lysis buffer (50 mM Tris, pH=7.5, 150 mM NaCl, 1 mM EDTA, 1 mM DTT, 1% Igepal CA-630) containing 1 pmol of IR700-25nt RNA (unmodified or cloaked) was incubated at 37 ˚C for 120 mins. Upon completion, all reactions were immediately mixed with 10 μL of RNA Gel loading dye (2×) and boiled at 95 ˚C for 2 mins. Samples were then resolved using 12% denaturing PAGE and imaged using a Li-Cor Odyssey imager in the 700 nm channel. The RNA integrity was calculated as the percentage of remaining intact RNA based on PAGE gel analyses.

Determine RNA enzymatic stability of EMX1-sgRNA. (Protection of RNA from RNase T1) 100 ng of EMX1-sgRNA (unmodified or cloaked, 2 μL of 50 ng/μL) was diluted with 6 μL of reaction buffer (50 mM Tris, pH=7.5 + 1 mM EDTA). To it was added 2 μL of a 5× solution of RNase T1 (0.5 U/μL) in 50 mM Tris, pH=7.5 containing 1 mM EDTA. The resulting solution was incubated at 37 ˚C for 9 mins. (Protection of RNA from FBS) 100 ng of EMX1-sgRNA (unmodified or cloaked, 2 μL of 50 ng/μL) was diluted with 8 μL 1×PBS, pH=7.4 containing 0.5% FBS (v/v). The resulting solution was incubated at 37 ˚C for 2 mins. Upon completion, the reaction mixture was immediately mixed with 10 μL of RNA Gel Loading dye (2×) and boiled at 95 ˚C for 2 mins. Samples were then resolved using 6% denaturing PAGE. The gel was stained with 1×SYBR Gold Nucleic Acid Gel Stain for 3 mins and imaged using a Typhoon 9410 gel scanner (Laser wavelength=488 nm). The images were visualized and processed using ImageStudioLite software.

Isolation of total cellular RNA. HEK293 cells were grown on 15-cm plates in DMEM supplemented with 10% FBS until 90% confluence. The cells were washed with 10 mL of PBS once, then resuspended in 500 μL of PBS and lysed with 6 mL of Trizol LS by vortexing. 1.2 mL of chloroform was then added. The resulting mixture was vortexed and incubated at room temperature for 5 mins, followed by centrifugation at 2500*g* for 15 mins at 4 ˚C. The aqueous phase was then mixed with 1× volume of 96% ethanol and purified using a Quick-RNA MidiPrep kit with gDNA digestion according to the manufacturer's protocol.

RT-qPCR analysis of isolated total cellular RNA. The reverse transcription was performed with isolated total cellular RNA with or without cloaking. As an internal control, 100 pg of eGFP-mRNA (5moU) was added to each 500 ng of cellular RNA immediately before reverse transcription. First, 1 μL of RNA (500 ng/μL) was mixed with 1 μL of 50 μM oligo$(dT)_{18}$ primer, 1 μL of 10 mM dNTP mix, and 10 μL of RNase-free water. The solution was incubated at 65 ˚C for 5 mins, then immediately cooled on ice for > 1 min. Next, 4 μL of RT buffer (5×), 1 μL of 0.1 M DTT, 1 μL of RiboLock, and 1 μL of SuperScript III (200 U/μL) were added to the solution. The reaction mixture was incubated at 50 ˚C for 60 mins and then terminated by heating at 70 ˚C for 15 mins. After cooling to 37 ˚C, 1 μL of RNase H (5 U/μL) was added. The resulting solution was then incubated at 37 ˚C for 20 mins and used for qPCR without further purification.

Next, the qPCR analyses were performed using Luna Universal qPCR Master Mix (NEB, M3003) on a StepOnePlus™ Real-Time PCR System. 1 μL of cDNA product was mixed with 10 μL of Luna Universal qPCR Master Mix, 1 μL of a solution containing 5 μM forward primer and 5 μM reverse primer, and 8 μL of water. Information about the primer sequences and amplicons for qPCR analyses of TBP, PPIE, and PSMB6 were listed in Supplementary Table 1 and 3. qPCR was performed using the following program: initial denaturation for 60 seconds at 95 ˚C; 40 cycles of alternating denaturation (15 seconds at 95 ˚C) and extension (30 seconds at 60 ˚C). ΔCt value was calculated to characterize the reverse transcription efficiency of each transcript as follows: the Ct value of each target was normalized to the Ct value of the internal control eGFP-mRNA (5moU) using the following equation: ΔCt (target) = Ct (target) - Ct (eGFP-mRNA (5moU)). ΔCt values were shown as mean ± s.e.m. (n=3 of three biologically independent experiments).

***In vitro* translation of eGFP-mRNA**. *In vitro* translation experiments were performed with eGFP-mRNA in Wheat Germ extract. 8 μL of 12.5 ng/μL eGFP-mRNA (100 ng in total) was added to a 384-well microplate (Greiner Bio-One, 781900). To it was added 12.5 μL of Wheat Germ extract (Promega, L4380), 0.5 μL of RNasin Plus RNase inhibitor (Promega, N2611), 2.0 μL of Complete AA mix (Promega, L4461), and 2.0 μL of 1 M KOAc. The resulting solution was mixed by gentle pipetting and then incubated at 25 ˚C for 90 mins. After incubation, the green fluorescence signal was measured using a Fluoroskan Ascent FL microplate fluorometer (Excitation:485 nm/Emission:538 nm).

Cas9-mediated dsDNA cleavage with EMX1-sgRNA. CRISPR-Cas9 experiments were performed with EMX1-sgRNA, PCR amplification products of genomic EMX1, and Cas9 nuclease. EMX1 dsDNA was generated by PCR amplification of the genomic EMX1 according to previously reported protocols[49] (see Supplementary Table 1 for related oligonucleotides sequences). 1 µL of 50 ng/µL EMX1-sgRNA was mixed with 5.67 µL of water, 1 µL of 10×NEbuffer 3.1, and 1.33 µL of 1 µM Cas9 Nuclease (*S. pyogenes*). The resulting solution was incubated at 25 ˚C for 10 mins. After incubation, 1 µL of 50 ng/µL of EMX1 dsDNA substrate was added and the reaction mixture was then incubated at 37 ˚C for 2 hours. After the reaction, 2 µL of 6×Orange Gel loading dye was added. The samples were resolved by electrophoresis on an 1% agarose gel containing 1×SYBR Gold Nucleic Acid stain. The gel was imaged using a Typhoon 9410 gel scanner (Laser wavelength= 488 nm). The gel images were visualized and processed using ImageStudioLite software.

Fluorescence-activated cell sorting (FACS) analyses of HeLa cells transfected with 4-cloaked eGFP-mRNA. HeLa cells were seeded on a 12-well plate and grown to ~40 % confluency in DMEM supplemented with 10% FBS in a humidified incubator at 37°C with 5% CO_2. Cells were transfected with 1 µg of eGFP-mRNA species per well using 3 µL of Lipofectamine MessengerMAX reagent according to the manufacturer's protocol. After 24 and 48 h, cells were washed once with warm DPBS and detached from wells by treatment with 100 µL of Trypsin-EDTA (0.25%). The cells were then mixed with 1 mL of DMEM, centrifuged at 350*g* for 5 mins. Next, the cells pellet was resuspended in 1 mL of 4% paraformaldehyde in PBS and fixed for 20 mins at 4 ˚C in the dark. Finally, the cells were centrifuged at 350*g* for 5 mins and resuspended in 180 µL of PBS containing 2% FBS. FACS analyses were performed on a NovoCyte Quanteon Flow Cytometer with a blue laser at 488 nm (100 mW) and a B530 detector. 25,000 cells were recorded per condition for analyses.

Confocal microscopy of eGFP-mRNA translation. HeLa cells were seeded onto a FluoroDish with a 10-mm cover glass bottom (World Precision Instrument, FD3510B100) at a density of 5.0×10^5 cells and incubated overnight in 100 µL of DMEM supplemented with 10% FBS at 37°C with 5% CO_2. Per FluoroDish, the cells were transfected with 100 ng of eGFP-mRNA species with 0.3 µL of Lipofectamine MessengerMAX transfection reagent according to the manufacturer's protocol. After 24 or 48 h, the medium was removed, then the cells were washed with PBS for three times and fixed with 200 µL of 4% paraformaldehyde for 20 mins at room temperature. After fixation, cells were washed with PBS for three times and then stained with 10 µg/mL Hoechst 33342 for 30 mins at room temperature. After staining, the cells were washed with PBS for three times, then mounted on an inverted Zeiss LSM 780 confocal laser scanning microscope equipped with a 34-channel spectral array with laser lines at 450 nm, 458 nm, 488 nm, 514 nm, 561 nm, 594 nm, and 633 nm in Cell Science Imaging Facility (CSIF) at Stanford University. A 25× oil immersive objective was employed for the imaging. Nucleus stained with Hoechst 33342 was imaged with a 405 nm laser with a 415–470 nm emission filter set, and GFP was imaged with a 488 nm laser with 500–615 nm. Images were processed and analyzed in ImageJ software.

Fluorimeter-based assays monitoring mRNA translation kinetics. On a 96-well plate, 0.01×10^6 of cells were seeded into each well in 100 µL of FluoroBrite DMEM (Thermo Scientific, A1896701) containing 10% FBS. In each well, cells were transfected by 100 ng of mRNA with 0.3 µL of Lipofectamine MessengerMAX reagent in serum-free FluoroBrite DMEM according to the manufacturer's protocol. Then, the transfection reagents were removed by replacing the medium with 180 µL of fresh FluoroBrite DMEM containing 10% FBS. GFP translation was monitored using a microplate reader (Tecan Infinite M1000) over time. GFP fluorescence was detected using 488 nm/519 nm for the excitation/emission wavelengths.

Quantification and statistical analysis. For all statistical tests (unless otherwise noted), a two-tailed Student's *t*-test was used to compare means between two samples. Significance is denoted as follows: * = $P< 0.05$, ** = $P< 0.01$, *** = $P< 0.001$, **** = $P< 0.0001$. Statistical tests were performed in GraphPad Prism9 software. Quantifications shown are mean ± s.e.m. unless otherwise stated.

Data availability

Data supporting the findings of this study are available in the article and Supplementary Information. Source data are provided with this paper. Data used for this paper are also available at https://doi.org/10.6084/m9.figshare.19555132.v1 at Figshare.

Acknowledgements

We acknowledge support from the U.S. National Institutes of Health (GM127295) for support of this work. We thank Kyle Fukui and other staffs at Stanford PAN facility for performing BioAnalyzer QC. We thank Stanford Shared FACS Facility (SSFF) for FACS service.

Competing interests

L.F and E.T.K have filed a provisional patent on the RNA cloaking and uncloaking reagents and methods described in this study.

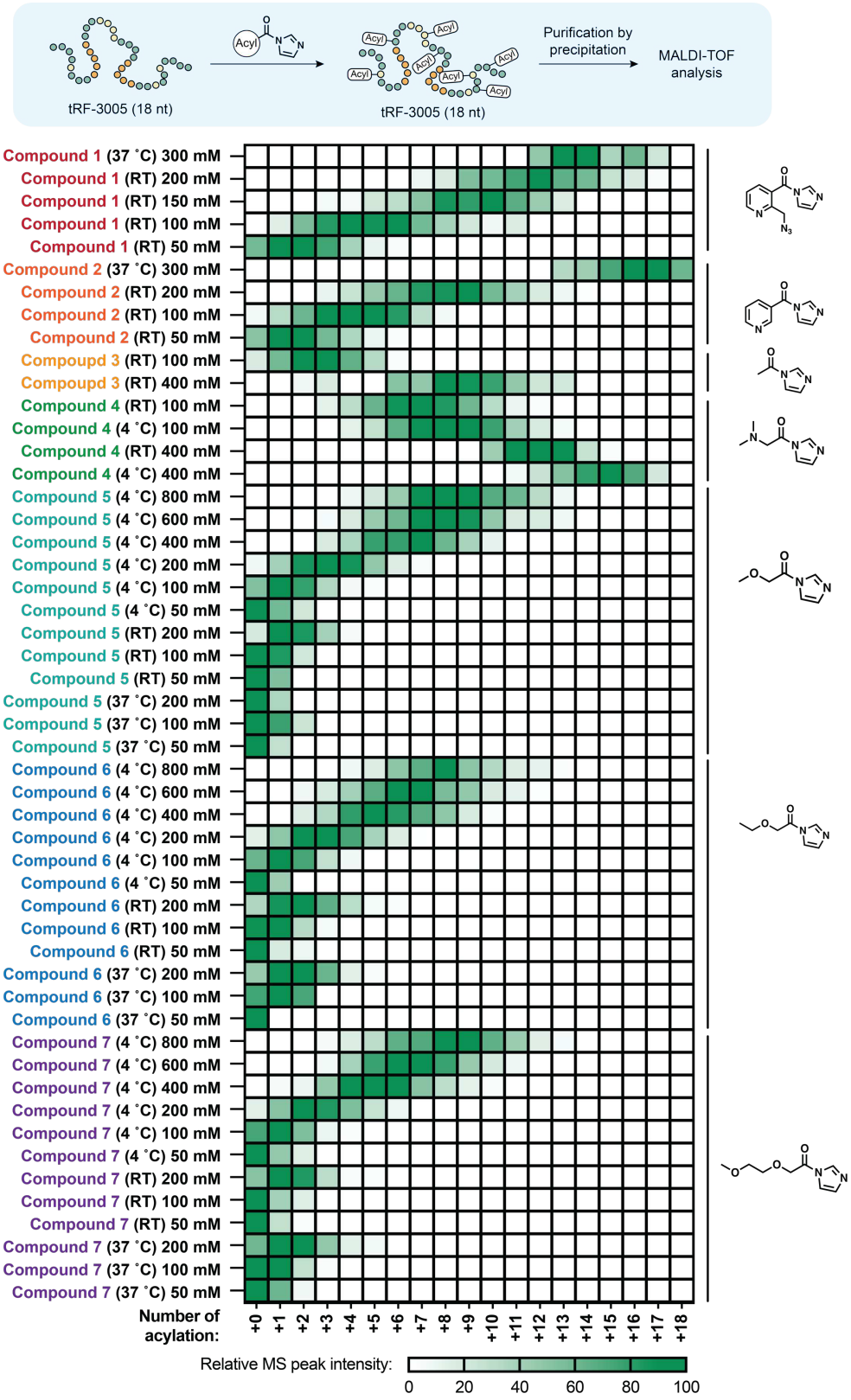

Extended Fig. S1 | Reaction conditions for each acylimidazole reagent (1-7) required to introduce the desired level of RNA cloaking using a model 18nt tRF-3005 RNA. The X-axis indicates the number of 2'-acyl adducts per RNA molecule identified by MALDI-TOF. The color intensity of each cell represents the mass intensity of the acyl adduct peak (numbers at bottom show numbers of acyl adducts for the model RNA strand).

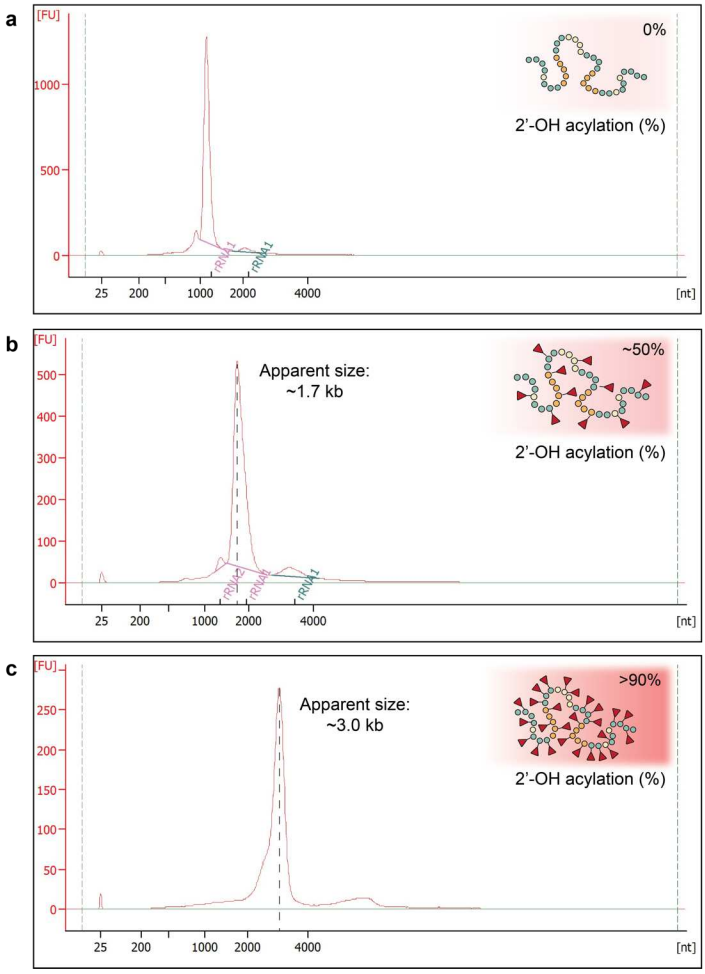

Extended Data Fig. S2 | RNA cloaking leads to reduced electrophoretic mobility of eGFP-mRNA and inflated apparent sizes during capillary electrophoresis analysis. **a**, Electrophoretic mobility of unreacted eGFP-mRNA determined by capillary electrophoresis analysis. **b**, Electrophoretic mobility of eGFP-mRNA with intermediate level (~50%) of cloaking by acylimidazole **1**. **c**, Electrophoretic mobility of eGFP-mRNA with extensive level (>90%) of cloaking by **1**. Capillary electrophoresis was performed on an Agilent BioAnalyzer 2100.

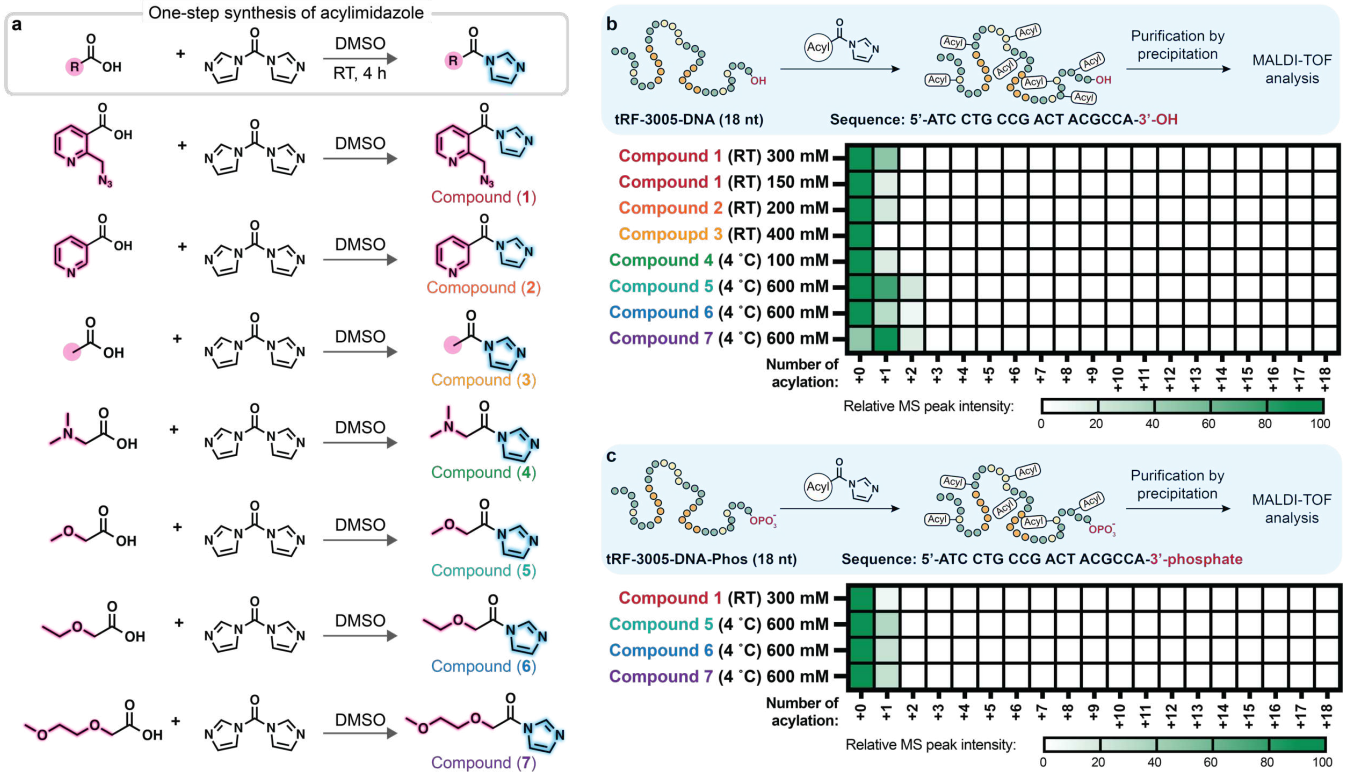

Extended Data Fig. S3 | One-step synthesis of acylimidazole reagents and their regioselective reactions with 2'-OH of RNA. a, Schematic for one-step synthesis of acylimidazole reagents. **b**-**c**, Comparisons of RNA and DNA with the same sequence (tRF-3005-DNA and tRF-3005-DNA-Phos) after reacting with **1**-**7** show that reaction occurs entirely or almost entirely at 2'-OH groups rather than nucleobases or phosphodiester bonds. **b**, Number of acyl adducts on tRF-3005-DNA (18nt) upon treatment with acylimidazole reagents **1**-**7**. tRF-3005-DNA contains an unmodified 3'-OH (Sequence: 5'-ATC CTG CCG ACT ACG CCA-3'-OH). **c**, Number of acyl adducts on tRF-3005-DNA-Phos (18nt) upon treatment with acylimidazole reagents **1**, **5**, **6**, and **7**. tRF-3005-DNA-Phos contains a blocked 3'-end by 3'-phosphorylation (Sequence: 5'-ATC CTG CCG ACT ACG CCA-3'-phosphate). The X-axis shows the number of acyl adducts per DNA identified by MALDI-TOF. The color intensity of each cell represents the mass intensity of the acyl adduct peak.

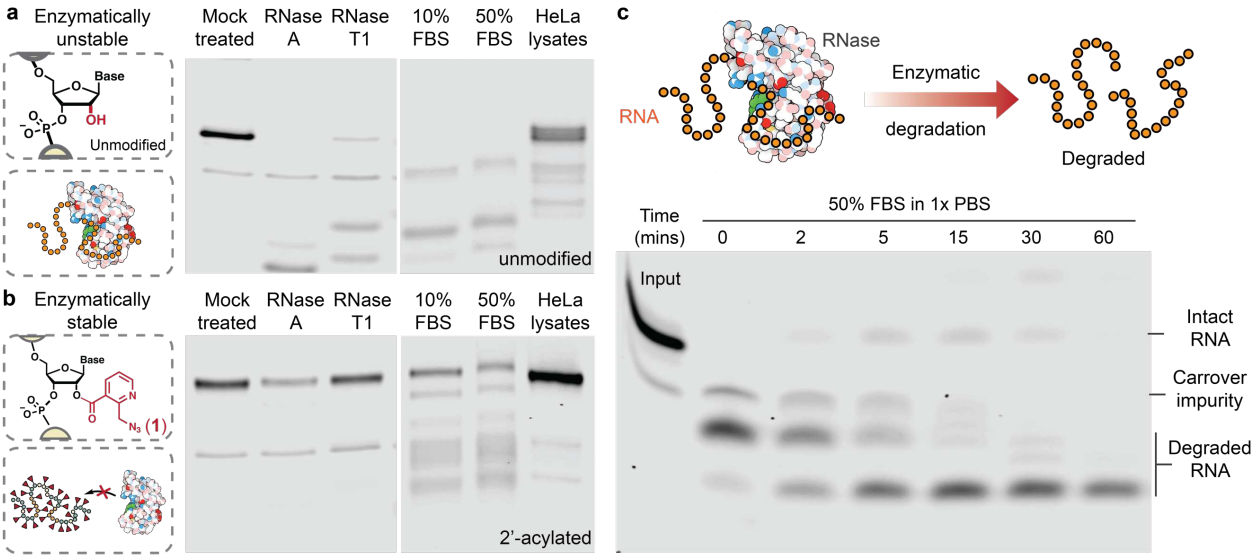

Extended Data Fig. S4 l Denaturing PAGE analyses showing the impacts of acylimidazole and level of cloaking on model IR700-RNA (25nt) degradation by RNases and biofluids. **a**-**b**, Representative PAGE gel showing the integrity of RNA without (**a**) or with (**b**) extensive cloaking with **1** after treatment with RNA degrading conditions. Experiments were performed three times. See Fig. 3c for statistical analysis. **c**, PAGE gel showing the integrity of model RNA upon treatment by 50% FBS.

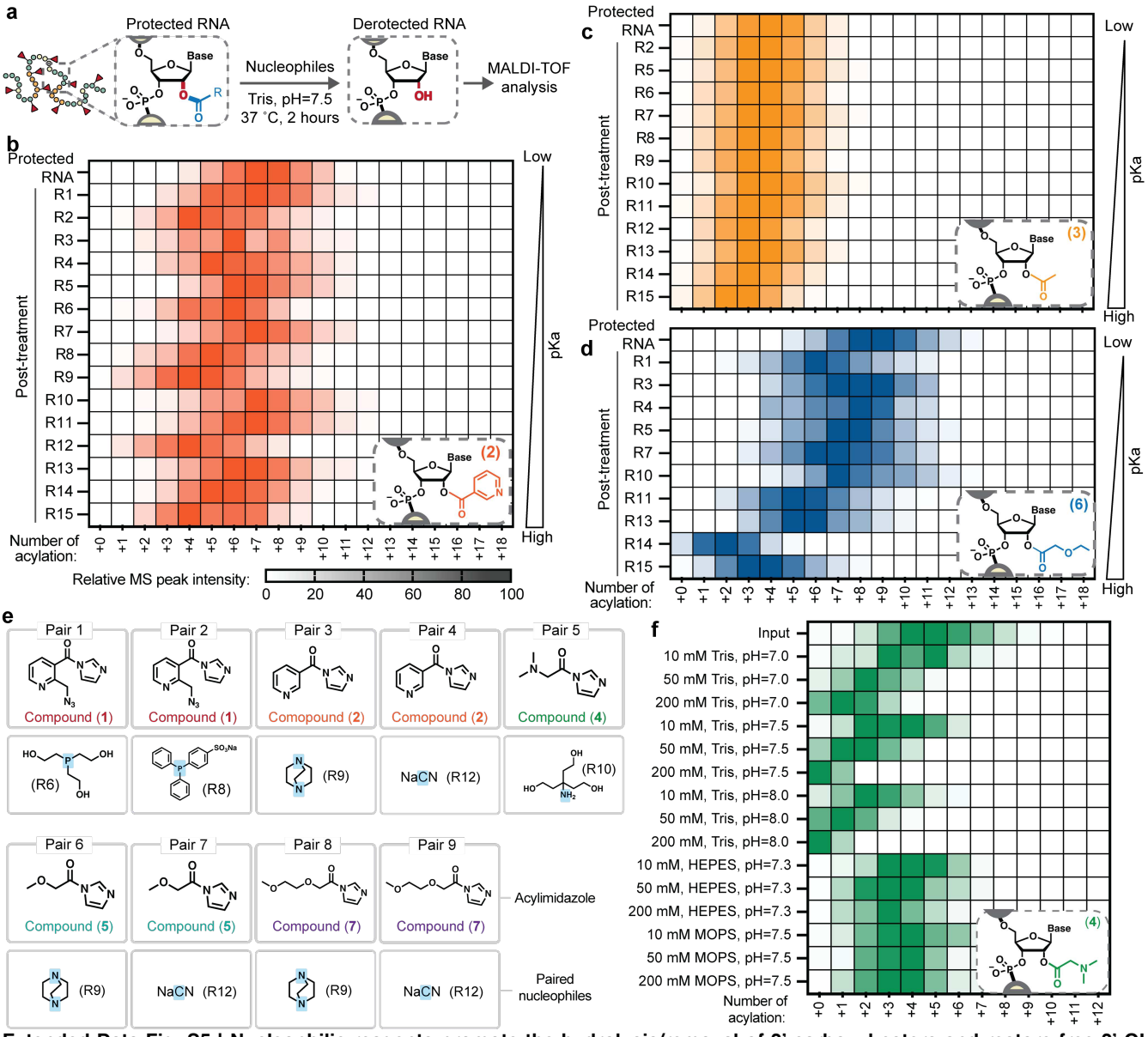

Extended Data Fig. S5 | Nucleophilic reagents promote the hydrolysis/removal of 2'-carboxyl esters and restore free 2'-OH groups at a neutral pH. a, Experimental workflow to test the efficiency of nucleophile-promoted hydrolysis of 2'-hydroxyl acylation. **b-d**, Nonbasic nucleophiles remove 2'-acyl adducts of tRF-3005 RNA installed by acylimidazole reagents **2** (**b**), **3** (**c**), or **6** (**d**) at differential rates. Cloaked tRF-3005 RNA was incubated with 50 mM of indicated nucleophiles in 50 mM Tris, pH=7.5 at 37 ˚C for 2 hours. MALDI-TOF analyses determined the average number of remaining 2'-acyl adducts on tRF-3005 RNA. See **Fig. 4b** for nonbasic nucleophiles used in this experiment. **e**, Sensitive acylimidazole-nucleophile pairs that afford >50% hydrolysis of 2'-acyl adducts within 2 hours. **f**, Heat map showing Tris selectively promotes the hydrolysis of 2'-acyl adduct by acylimidazole reagent **4**.

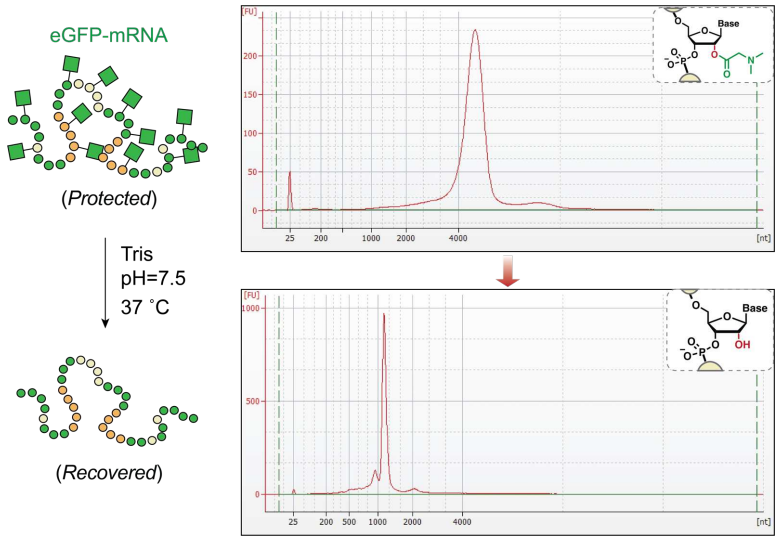

Extended Data Fig. S6 | eGFP-mRNA remains nearly fully intact after treatment by 50 mM Tris, pH=7.5 at 37 ˚C for 24 h. RNA fragment analysis by capillary electrophoresis determines the integrity of **4**-cloaked eGFP-mRNA before and after treatment with 50 mM Tris, pH=7.5 without the addition of RNase inhibitors. Capillary electrophoresis was performed on an Agilent BioAnalyzer 2100.

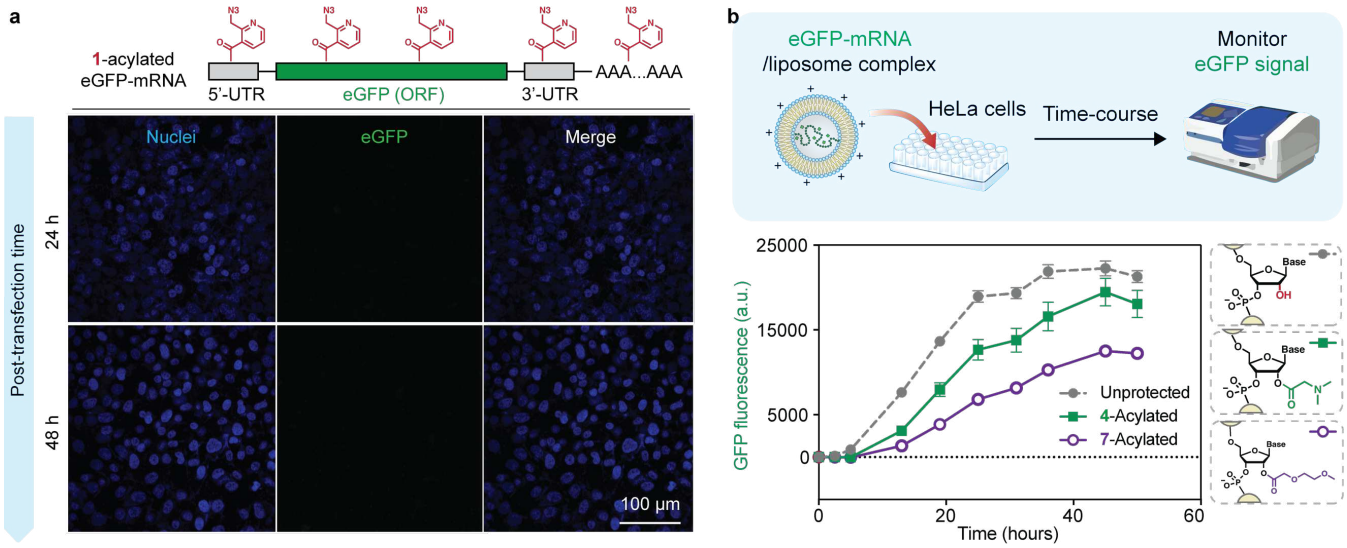

Extended Data Fig. S7 | Spontaneous release of 2'-esters restores mRNA translation in human cells. **a**, Representative single-blind fluorescence micrographs of HeLa cells transfected with **1**-cloaked eGFP-mRNA showing strongly inhibited mRNA translation after 24 or 48 h. **b**, Time-course plot showing **7**-cloaked eGFP-mRNA (~50% of 2'-hydroxyls acylated) translates in HeLa cells. Its translation kinetics were compared to unprotected or equimolarly **4**-cloaked eGFP-mRNA. Data represent mean ± s.e.m., *n*=3 per group from three biologically independent experiments.

Supplementary Files

This is a list of supplementary files associated with this preprint. Click to download.

- SIfangkool.pdf